ACS OMEGA

http://pubs.acs.org/journal/acsodf

Article

Isolation, Expansion, and Characterization of Placenta Originated *Decidua Basalis*-Derived Mesenchymal Stromal Cells

Priya Subramani, Jaianand Kannaiyan, Jothi Ramalingam Rajabathar, Prema Paulpandian, Ramesh Kumar Kamatchi, Balaji Paulraj, Hamad A. Al-Lohedan, Selvaraj Arokiyaraj, and Veeramanikandan Veeramani*

Cite This: *ACS Omega* 2021, 6, 35538−35547

Read Online

ACCESS | Metrics & More | Article Recommendations

ABSTRACT: Mesenchymal stromal cells (MSCs) were isolated from *Decidua Basalis* (DB) and studied for their final cellular product measures, such as safety, purity, quality, quantity, and integrity that are ascribed as cellular products. This research aimed to isolate MSCs for expansion under the clinical scale level with potency, secretion of cytokines, growth factors secreted by DB-MSCs, and their role in wound healing. Placentas isolated from DB were expanded up to the 10th passage, and their characteristics were assessed by phenotypic characterization using a flow cytometer and analyzed for trilineage differentiation by cytochemical staining. Growth factors (GF), interleukins (IL), chemokines, and tissue inhibitors of metalloproteinases (TIMP) were measured with enzyme-linked immunosorbent assays. The harvested cells from the placenta yield 1.63−2.45 × 10^4cells/cm^2 at P(0), 3.66−5.31 × 10^4cells/cm^2 at P(1), 4.01−5.47 × 10^4cells/cm^2 at P(2), and 3.94−5.60 × 10^4cells/cm^2 at P(10) accordingly; up to 4.74 × 10^9 P(2) DB-MSCs were harvested within 9−11 days. The viability of the freshly harvested cells was greater than 90% in all cases. It is able to differentiate into chondrocytes, adipocytes, and osteogenic cells, proving their ability to differentiate into a trilineage. Thus, this study put an insight into a secure and conventional approach toward their ability to differentiate into multiple lineages and secrete factors related to immune regulation, making DB-MSCs a potential source in various therapeutic applications.

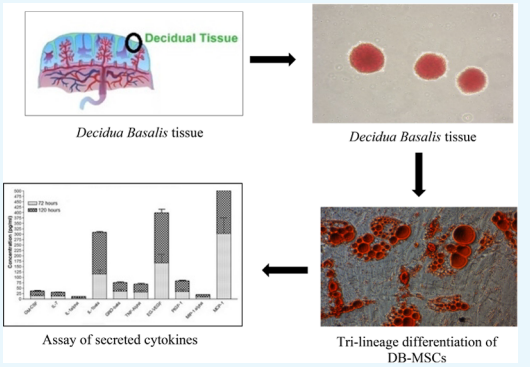

INTRODUCTION

Wound healing is accomplished through cellular homeostasis, inflammation, proliferation, and tissue remodeling by total physical and functional regeneration of injured tissue.[1−3] Furthermore, these metabolic processes are controlled by extracellular signaling pathways such as cytokines, growth factors, and membrane receptors.[4,5] However, wound curing is a usual biological process; chronic wound treatment frequently necessitates therapeutic intervention to provide a biochemical environment that promotes normal healing. To treat and control the complicated pathophysiology of chronic wounds, many therapeutic modalities are already available.[6] Among those, biophysical practices like electro-physical stimulation, recombinant growth factor therapy, platelet rich plasma treatment, and stromal cell based treatment are very common.[7,8] Particularly, the wound healing process is a multimodal strategy that stimulate signaling response; then, the replacing growth factors or targeting particular processes like angiogenesis or proliferation are more likely to provide therapeutic advantages.

Placental membranes, the earliest known biomaterials utilized for wound healing, are one such technique. Placental membranes have been shown to have good clinical effectiveness as well as a minimal treatment cost.[9] Extra-embryonic tissue gives rise to placental membranes. A fetal component (the chorionic plate) and a maternal component (the *Decidua Basalis*) make up this tissue.[10−12] Human-derived *Decidua Basalis* has been found to help heal chronic wounds in riffle clinical trials and recent *in vitro* investigations due to their capacity to produce cytokines and impact on cell propagation, angiogenesis, and exodus.

Here, we optimized the utilization of *Decidua Basalis*-derived mesenchymal stromal cells (DB-MSCs) for wound healing and therapeutic purposes, which, on the other hand, is dependent on their subsequent large-scale *in vitro* growth. To address clinical demand and biological research demands, a rapid and effective methodology for producing large amounts of DB-

Received: September 15, 2021
Accepted: December 6, 2021
Published: December 16, 2021

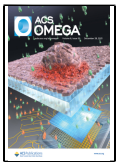

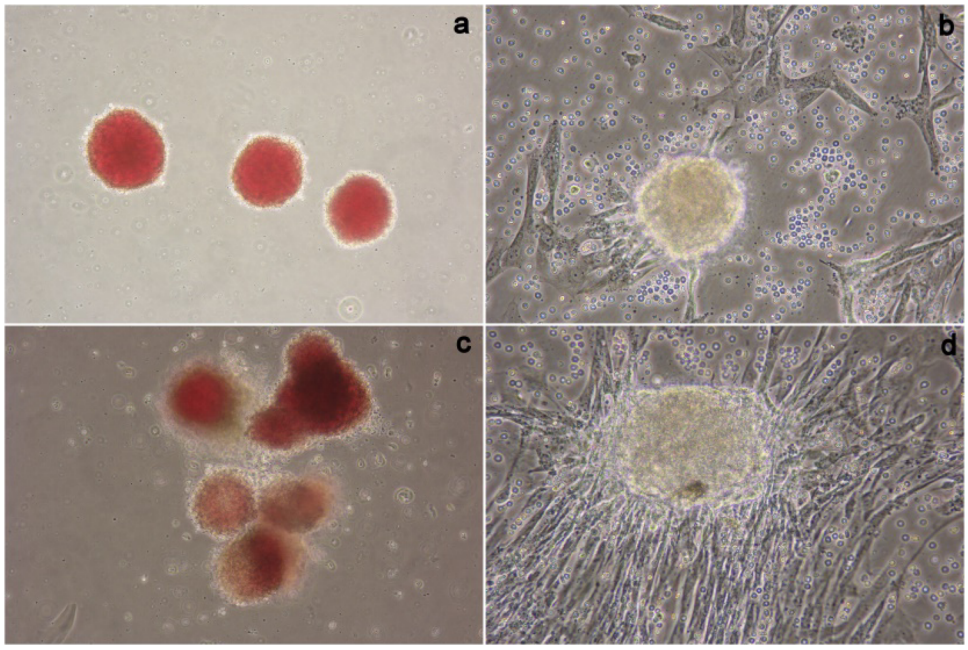

Figure 1. Morphology and growth of the cells at the primary passage level. (a) *Decidua* tissue explants seeded after 36 h, (b) escalation of cells from explant after 72 to 84 h, (c) seeded explants after 48 h, and (d) escalation of cells from explant after 120 h of *Decidua Basalis* samples (magnification, 10×).

MSCs is necessary. Furthermore, well-characterized cell lines that continue to proliferate while preserving their characteristic features are extremely useful in research. We looked into DB-MSC expansion on a clinical scale up to 10 passing levels. The cells' development was monitored from the first 24 h to 10th passages. The phenotypic characterization of DB-MSCs was performed using a flow cytometer labeled with antibodies against human antigens CD79 (PE), CD 14 (APC), CD19 (PE), CD133 (PE), CD34 (PE), CD45 (PE), human leucocyte antigen-DR (PE), and CD79 (APC) as negative markers and CD73 (APC), CD90 (FITC), CD166 (PerCP-Cy5.5), and CD105 (PerCP-Cy5.5) as specific markers; expanded DB-MSCs were also analyzed for differentiation into all trilineage using cytochemical stain. We also quantified the array of growth factors, interleukins (ILs), chemokines, and tissue inhibitors of metalloproteinases (TIMPs) existing in the *Decidua Basalis*-derived mesenchymal stromal cells homogenates.

Taken together, our findings show that DB-MSCs being expanded on a massive scale for clinical and therapeutic purposes were evidenced that majority of the cells had adhered to the flask and had transformed into fibroblast-like cells with a spindle in the entire passage levels. The physiologic features of DB-MSCs, such as plastic adherence, shape, specific surface antigens, and multipotent differentiation capacity, have been demonstrated by clinical-grade expansion. As indicated by the continuously collected cell density following clinical-scale growth, cell size did not vary significantly. We further evaluated the profiling of cytokines secreted by *Decidua Basalis*-derived mesenchymal stromal cells.

RESULTS

Growths of the cells were observed after 120 h, at which time the cells were mostly on all sides of flasks and elliptical. After 120 h incubation, with media change once, most of the cells started to extend to the flask and became fibroblast-like cells and spindle in shape (Figure 1), and the uniform morphology was retained until the 10th subsequent passaging.

Approximately 9.8−14.7 × 10^6 cells were detached initially from the *Decidua Basalis* (n = 5) at the end of passage 0 after 14−18 days. After 24 h of seeding, fibroblastic morphology was observed with adherent cells. The cells were trypsinized and implanted into 3000 cells/cm^2 in T-175 flasks. Adherent cells were harvested after the confluence of cell populations attained 1.2−2.6 × 10^8. DB-MSCs were acquired in 9−11 days after the successive passages with a 1:3 split ratio (1.60−4.74 × 10^9 P(2)). The cells were cryopreserved at the end of the first expansion period. The freshly harvested cells sustainability was better than 90% in all occasions. The present method yields 1.63−2.45 × 10^4cells/cm^2 at P(0), 3.66−5.31 × 10^4 cells/cm^2 at P(1), 4.01−5.47 × 10^4cells/cm^2 at P(2), and 3.94−5.60 × 10^4cells/cm^2 at P(10) consequently from *Decidua Basalis* placenta. On the whole, the collection, processing, and harvesting of the *Decidua Basalis* sample are illustrated in Figure 2. The surface markers of MSCs were identified with FACs analysis at the 2nd and 10th passages. The cell cultures were displayed to be free from hematopoietic cell lineage markers such as CD79, CD14, CD19, CD133, CD45, CD34, and HLA-DR. However, a maximum expression of CD73, CD90, CD166, and CD105 was observed for all populations.

In all of the culture conditions investigated in the studies, there was no visible change in the multi-lineage differentiation capability of *Decidua Basalis* generated MSCs toward adipogenic, chondrogenic, or osteogenic lineages. Figure 3 shows that MSCs derived from *Decidua Basalis* preserved their capability to develop into adipocytes, chondrocytes, and osteoblasts. After 21 days of induction, tiny fat droplets in the cytoplasm indicated adipogenic differentiation (Figure 3B). The shape of the induced cells eventually grew bigger and expanded. The presence of oil red-stained lipid droplets in the cytoplasm of cells are considered as positive, whereas in control cells, no fat droplet was observed (Figure 3A), and the

https://doi.org/10.1021/acsomega.1c05022
ACS Omega 2021, 6, 35538−35547

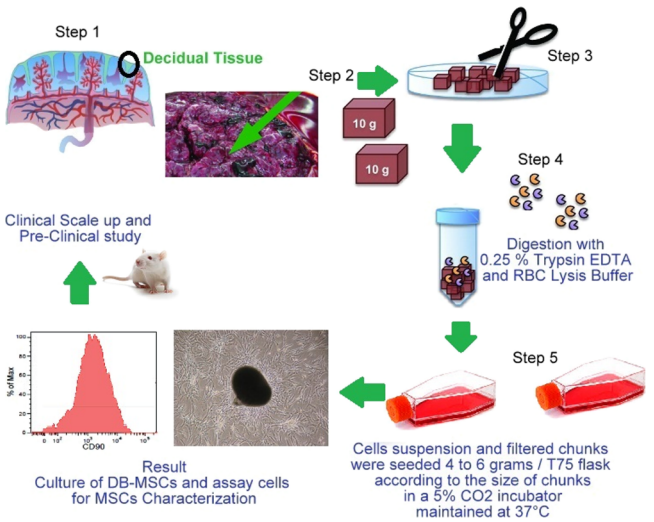

Figure 2. Collection, processing, and harvesting of *Decidua basalis*.

number of stained cells grew in a time-dependent way. For osteogenic differentiation , in an inducing culture media, *Decidua Basalis* cells started to change their morphology as soon as 7 days of osteogenic differentiation and cells were extinct their fibroblast appearance and became a spherical and cuboidal form. The potential DB-MSCs were developed into osteocytes under osteogenic differentiation; they were identified with strong black stain between osteogenic cells (Figure 3D); and no calcium deposition was observed in cells under control conditions (Figure 3C). Chondrocyte differentiation, MSCs were positively distinguished into chondrocytes as shown in Figure 3F, and the cells were labeled safranine O stained patches/pellets. No changes were observed with undifferentiated or control cells (Figure 3E).

The difference between each set of pairs and their differences were analyzed for 72 and 120 h with cytokine values using the Wilcoxon test. The statistical difference of the cytokines/chemokines/growth factors M-CSF, IL-7, IL-1alpha, IL-1beta, GRO-beta, TNF-alpha, EG-VEGF, PIGF-1, MIP-1alpha, MCP-1, ICAM-1, CTGF, CXCL 16, and RANTES

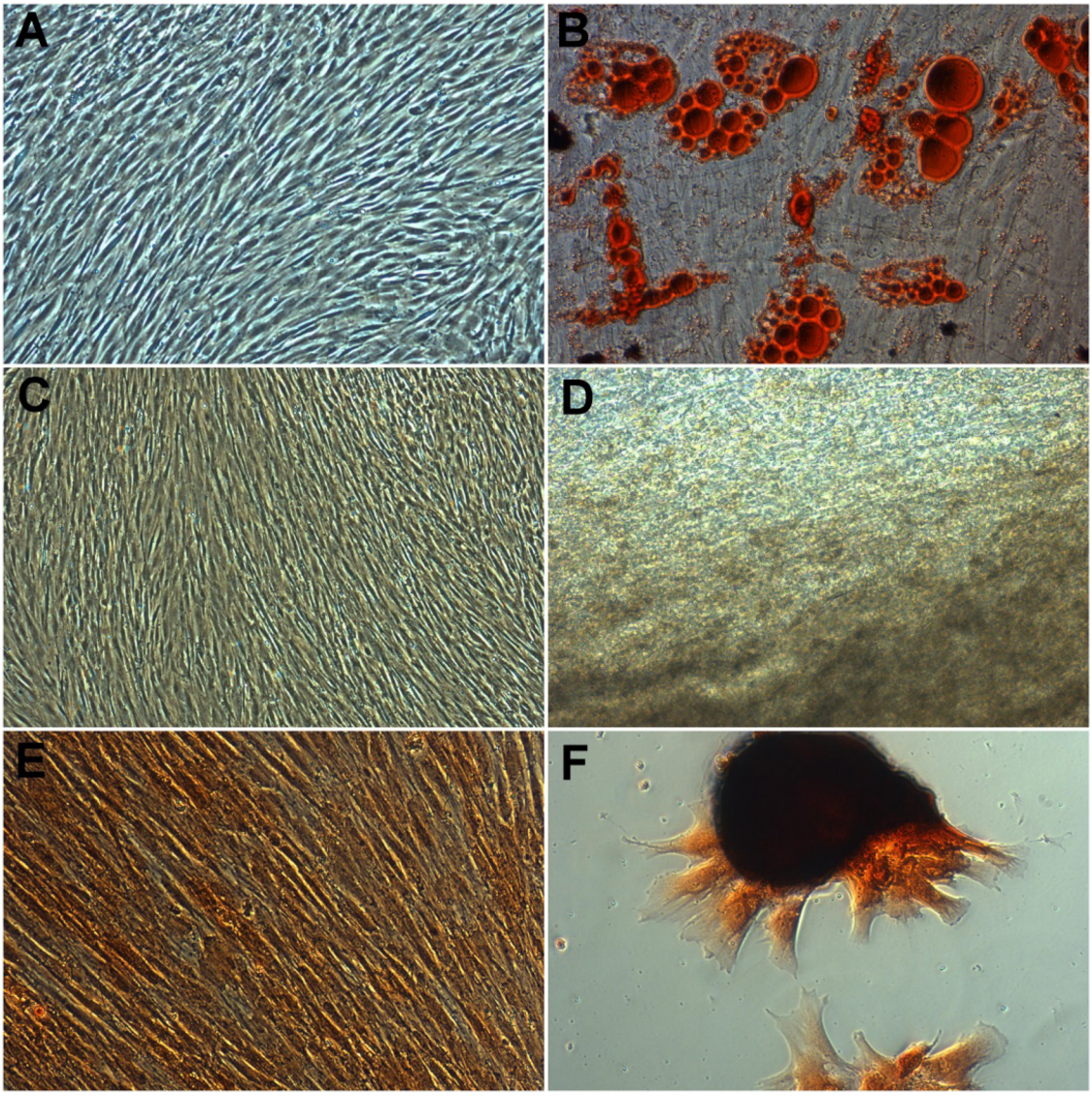

Figure 3. Tri-lineage differentiation of DB-MSCs retained their capacity to differentiate into adipocytes (B), osteoblasts (D), and chondrocytes (F). No changes were observed in undifferentiated or control cells (A, C, E) (magnification, 10×).

https://doi.org/10.1021/acsomega.1c05022
ACS Omega 2021, 6, 35538−35547

Table 1. Wilcoxon Signed Ranks Test

	72 h						120 h					
cytokine profile	*N*	mean	std deviation	minimum	maximum	*P*-value	*N*	mean	std deviation	minimum	maximum	*P*-value
GM-CSF	5	15.50	3.76	11.49	21.27	**0.043**	5	21.39	3.66	17.04	26.59	**0.043**
IL-7	5	14.19	3.44	10.52	19.47	**0.043**	5	16.89	3.39	13.06	21.91	**0.043**
IL-1alpha	5	4.94	0.91	3.97	6.26	**0.043**	5	6.23	0.84	5.24	7.42	**0.043**
IL-1beta	5	114.71	19.32	97.00	143.70	**0.043**	5	192.54	9.79	177.91	200.00	**0.043**
GRO-beta	5	36.11	8.77	26.76	49.56	**0.043**	5	39.07	8.71	29.55	52.23	**0.043**
TNF-alpha	5	32.65	7.93	24.20	44.81	**0.043**	5	35.66	7.87	27.03	47.53	**0.043**
EG-VEGF	5	166.04	40.35	123.06	227.89	**0.043**	5	231.36	39.15	184.60	286.80	**0.043**
PIGF-1	5	35.49	8.62	26.30	48.71	**0.043**	5	47.18	8.40	37.32	59.25	**0.043**
MIP-1alpha	5	8.13	1.98	6.02	11.16	**0.043**	5	11.10	1.92	8.82	13.83	**0.043**
MCP-1	5	301.80	73.33	223.68	414.22	**0.043**	5	421.95	71.15	336.88	522.59	**0.043**
ICAM-1	5	424.83	103.23	314.87	583.09	**0.043**	5	506.48	101.51	391.79	656.73	**0.043**
CTGF	5	22.02	5.35	16.32	30.22	**0.043**	5	30.79	5.19	24.58	38.13	**0.043**
CXCL 16	5	5.83	1.42	4.32	8.00	**0.043**	5	8.15	1.37	6.51	10.09	**0.043**
RANTES	5	69.86	16.98	51.78	95.89	**0.043**	5	85.46	16.65	66.48	109.96	**0.043**

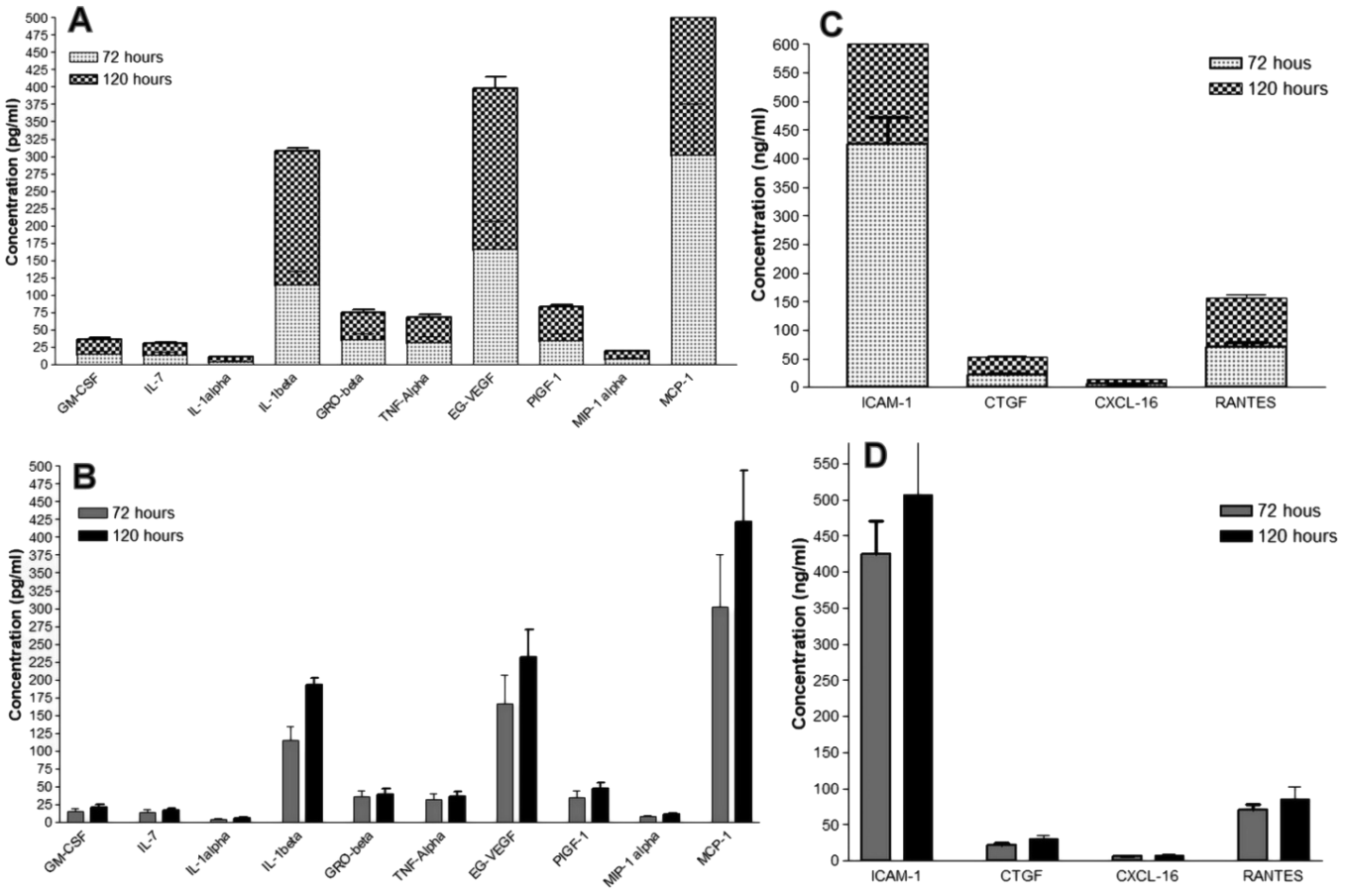

Figure 4. The secreted cytokine concentrations expressed in pg/ml for GM-CSF, IL-7, IL-1alpha, IL-1beta, GRO-beta, TNF-alpha, EG-VEGF, PIGF-1, MIP-1alpha, and MCP-1 were evaluated. Similarly, the secreted chemokine and growth factors concentrations expressed in ng/ml for ICAM-1, CTGF, CXCL-16, and RANTES were evaluated using cytokine profiling, where (A, C) stack column statistical analysis is expressed as mean SEM, while (B, D) interleaved column statistical analysis is expressed as mean SD.

involved in wound healing and secretion concentration in 72 h and 120 h was tested for the null hypothesis between the two populations and is tabulated in Table 1. The Wilcoxon signed-rank test infers that the null hypothesis of 72 and 120 h was found with the same continuous distribution. The significant values that are observed for both populations are $P < 0.043$, and it is mathematically significant.

The data of cytokine profiling are analyzed for the secreted cytokine concentrations in pg/ml for the cytokines GM-CSF, IL-7, IL-1alpha, IL-1beta, GRO-beta, TNF-alpha, EG-VEGF, PIGF-1, MIP-1alpha, and MCP-1. The expression for stacked column statistical analysis was expressed as mean ± SEM (Figure 4A), and interleaved column statistical analysis was expressed as mean ± SD (Figure 4B). For the column statistics of 72 h, the minimum value was 4.9 pg/mL and the maximum

https://doi.org/10.1021/acsomega.1c05022
ACS Omega 2021, 6, 35538−35547

value was 300 pg/mL, with a mean of 73 pg/mL SD 96 of SD error 30. The *P*-value (two-tailed) is 0.0395; it is arithmetically significant. Similarly, for the column statistics of 120 h, the minimum value was 6.2 pg/mL and the maximum value was 420 pg/mL, with a mean of 100 pg/mL SD 140 of SD error 43. The *P*-value (two-tailed) is 0.0429, and the value is statistically significant. The data for selected cytokine profiling are analyzed for the secreted cytokine concentrations in ng/mL for the cytokines ICAM-1, CTGF, CXCL 16, and RANTES. The expression for stacked column statistical analysis was expressed as mean ± SEM (Figure 4C), and interleaved column statistical analysis was expressed as mean ± SD (Figure 4D). For the column statistics of 72 h, the minimum value was 5.8 ng/mL and the maximum value was 420 ng/mL, with a mean value of 130 ng/mL SD 200 of SD error 99. *P*-value (two-tailed) is statistically significant. Correspondingly, for the column statistics of 120 h, the minimum value was 8.2 ng/mL and the maximum value was 510 ng/mL, with a mean value of 160 ng/mL SD 230 of SD error 120. The *P*-value of the one-sample *t*-test (two-tailed) is statistically significant ($P < 0.05$).

Table 1 shows the comparison level of the secreted cytokines in two different period intervals of 72 and 120 h. All the cytokines/chemokine/growth factors in 72 and 120 h were statistically significant. The concentration of secreted cytokines/chemokines/growth factors in 72 and 120 h was analyzed by a correlation method. Data were expressed as mean (ng/mL/pg/mL) ± SEM. Statistical significance between groups was determined using the paired non-parametric Wilcoxon test. The *P*-values in bold indicate statistically significant ($p < 0.05$) values.

DISCUSSION

Wound healing necessitates a synergistic interaction between cells, growth factors, and extracellular matrix proteins. The endogenous mesenchymal stromal cell (MSC) strikes at the core of this process, regulating the repair response by recruiting other host cells and secreting growth factors and matrix proteins. MSCs are self-renewing multipotent stromal cells with the ability to develop into a variety of mesenchymal lineages, including bone, cartilage, tendon, and fat. MSCs control immune response and inflammation, as well as possess significant tissue-protective and reparative processes, making them appealing for the treatment of a variety of illnesses. Exogenous MSCs have been shown to have a positive effect on wound healing in several animal models and clinical situations. They have been used to treat chronic wounds and jumpstart delayed healing processes, to name a few applications. Human placental membranes are a rich source of MSCs for tissue regeneration and repair, as per recent research.

Recent translational research initiatives have made success in developing innovative strategies for stem cell administration into healed wounds utilizing contemporary bioengineering methods. To achieve the maximum therapeutic effect, MSCs engraftment in cutaneous wounds and clinically proven large-scaled MSCs must be optimized. The delivery procedures, wound models, and MSCs populations used in published research differ significantly, making it difficult to assess the influence of delivery time, quality and quantity of cells demanded, number of cells supplied, and delivery location on MSCs engraftment.

With recent progress in MSCs-based treatment, there are still a few obstacles to overcome before MSCs can be utilized to treat wounds effectively. The disparity in MSCs surface receptor expression and behavior within and across studies highlights the significance of uniform criteria for defining MSCs, uniform procedures for isolation and growth, cytokine levels, cell proliferation, migration, and secretion of endogenous cytokines to prove their identity before therapeutic delivery. Only a few studies have been conducted to substantiate the therapeutic potential of DB-MSCs in human; although the results are promising, they are limited by small sample sizes, short follow-up periods, and a limitation of randomized controlled trials. Several studies are presently enrolling participants to study the long-term effects of bone marrow MSCs treatment on diabetic and venous ulcers. However, understanding the rising clinical use of DB-MSCs is still unfolding and it depends only on the development of large-scale MSCs productions and the complete profiling of cytokines and growth factors.

At this point, the ultimate cellular product must fulfill the many controlling standards for cell therapy products, *i.e.*, safety, integrity, strength, purity, and quality. We optimized the massive production of DB-MSCs for clinical and therapeutic applications in this investigation. Plastic adherence, shape, particular surface antigens, and multipotent differentiation capacity of DB-MSCs were all intact upon clinical-large scale multiplication. The cells were found to be a homogeneous spindle-like monolayer. As indicated by the continuous harvested cell density following clinical-scale growth, cell size did not vary significantly. In P(2) we were able to grow to generate as many as 4.74×10^9 cells from a distinct placenta unit, as well as observe viability, acaulescent, and karyotyping up to P(10) with no prominent changes in capability, acaulescent, or karyotyping. Colony-forming unit (CFU) analysis studies revealed the growth rate and the ability of the cell in the population to undergo "unlimited" division of DB-MSCs.

Flow cytometry indicated that antibodies against CD73, CD90, CD166, and CD105 responded with more than 90% of the cells, whereas antibodies against CD79, CD14, CD19, CD133, CD45, CD34, and HLA-DR responded with less than 3% of the cells. In an overview, immuno-phenotype analysis revealed that DB-MSCs were progressive for MSC markers like CD73 (98.99−99.93%), CD90 (94.44−97.63%), CD166 (98.11−99.75%), and CD105 (98.11−99.75%) (96.71−99.40%). MSCs have a distinctive form of cell surface antigens, containing CD73, CD90, and CD105. CD79 (0.58−0.45%), CD14 (2.54−0.24%), CD19 (0.96−0.59%), CD133 (1.50−0.07%), CD34 (0.45−0.10%), CD45 (0.23−0.08%), and HLA-DR are antigens that are not typically present on MSCs (0.38−2.34%). These cells were identified to exhibit an immuno-phenotype related to MSCs and to be proficient on self-renewal. Furthermore, until P(10), the rate of DB-MSC proliferation remained constant.

These cells' capacity to distinguish into osteogenic, chondrogenic, and adipogenic lineages was established, paving the way for their use as a viable healing tool to fulfill rising remedial needs. To confirm the DB-MSCs' adipogenesis potential, after 21 days of induction, tiny fat droplets in the cytoplasm could be seen, indicating adipogenic differentiation. Induced cells grew in size and increased cell shape with time. A number of stained cells were raised in a time-dependent way as lipid droplets labeled with oil red accumulation in the cytoplasm of positive cells (Figure 3B). In the control group, however, no fat droplet was seen (Figure 3A). In an inducing culture media, cells began to alter structurally as soon as 7 days

https://doi.org/10.1021/acsomega.1c05022
ACS Omega 2021, 6, 35538−35547

Table 2. Cytokine Profiling of *Decidua Basalis*-Derived Mesenchymal Stem Cells

name of cytokine/growth factors	systematic name	function/category	assay range	sensitivity	values reported in literature studies	recovered values	primary Function in wound healing
GM-CSF	granulocyte colony stimulating factor	proliferative cytokine	7.8−500 pg/mL	7.0 pg/mL	10 pg/mL	17.04−26.59 pg/mL	improves wound healing either directly or indirectly by activating secondary cytokines like TGF1. Regulating angiogenesis development, cellular responses, and tissue remodeling directly through its mitogenic action for keratinocytes and the stimulation of endothelial cell proliferation and migration ([16,17])
IL-7	interleukin 7	hematopoetic growth factor	3.9−250 pg/mL	3.0 pg/mL	20 ng/mL	13.06−21.91 pg/mL	IL-7 is a pleomorphic cytokine that has previously been demonstrated to boost epidermal T-cell proliferation and survival in normal human keratinocytes. It has a key function in immune development, including early B- and T-cell development as well as peripheral T-cell homeostasis. IL-7 expression was increased in all levels of the epidermis during the healing of chronic wounds ([18,19])
ICAM-1	intercellular adhesion molecule	pro-inflammatory cytokine	15.6−1000 ng/mL	15.0 ng/mL	nil	391.79−656.73 ng/mL	ICAM-1 is a transmembrane protein associated with endothelial cells and leukocytes that has long been recognized for its role in cell−cell interactions and leukocyte-endothelial transmigration ([20])
IL-1α	interleukin I alpha	pro-inflammatory cytokine	3.9−250 pg/mL	3.0 pg/mL	1.7 ng/mL	5.24−7.42 pg/mL	they have an impact on the inflammatory phase ([17,21])
IL-1beta	interleukin 1 beta	pro-inflammatory cytokine	3.9−200 pg/mL	3.9 pg/mL	20 ng/mL	177.91−200.00 pg/mL	They aid wound healing by limiting proliferation ([17,22]).
human CTGF	human connective tissue growth factor	growth factor	3.9−250 ng/mL	3.0 ng/mL	10 ng/mL	24.58−38.13 ng/mL	Chemotaxis stimulation, fibroblast proliferation, and extracellular matrix protein induction, including fibronectin and collagen type I. CTGF expression in the skin is linked to myofibroblast induction, and CTGF-expressing pericytes play a key role in myofibroblast activity during cutaneous tissue regeneration ([17,23])
human GRO-beta	humum growth-related oncogene	chemokines	3.9−250 pg/mL	3.0 pg/mL	60 pg/mL	29.55−52.23 pg/mL	GRO-beta (growth-regulated oncogene) or CXCL2 is a member of the CXC family of proteins that play a key role in neutrophil and basophil recruitment and activation in response to tissue damage and microbial infection. GRO-beta is found in epithelial cells, monocytes, fibroblasts, and melanocytes, and it is activated during inflammatory, epithelialization, and angiogenic processes, such as the healing of human burn wounds ([20,24])
human TNF-alpha	human tumor necrosis alpha	pro-inflammatory cytokine	7.8−500 pg/mL	7.0 pg/mL	10 ng/mL	27.03−47.53 pg/mL	TNF- promotes wound epithelialization and neovascularization. TNF- seems to have a direct influence on wound healing and can compensate for the detrimental effects of macrophage decrease ([25,26])
CXCL 16	C-X-C motif chemokine 16	chemokines	3.9−250 ng/mL	3.0 ng/mL	nil	6.51−10.09 ng/mL	proangiogenic factor (promote angiogenesis) ([27])
human EG-VEGF	human endocrine gland derived vascular endothilial growth factor	angiogenic growth factor	15.6−1000 pg/mL	15.0 pg/mL	128.5 pg/mL	184.60−286.80 pg/mL	proangiogenic prokineticin 1 (promote angiogenesis) ([21,27])
CCL5 /RANTES	chemokine (C−C motif) ligand 5	chemokines	7.8−500 ng/mL	7.0 ng/mL	30 pg/mL	66.48−109.96 ng/mL	chemoattractants for monocytes/macrophages in normal (acute) skin wound healing ([20,24])
human PIGF-1	human placental growth factor	pleiotropic cytokine	3.9−250 pg/mL	3.0 pg/mL	10 ng/mL	37.32−59.25 pg/mL	during cutaneous wound healing, placenta growth factor (PlGF), an angiogenic mediator that promotes pathologic neovascularization, is produced and facilitates wound closure by increasing angiogenesis. Growth and migration are aided by PIGF ([28,29])
MIP-1alpha	macrophage inflammatory protein 1-alpha	chemokines	3.9−250 pg/mL	3.0 pg/mL	1-10 ng/mL	8.82−13.83 pg/mL	MIP-1α and MIP-1β promote wound closure. MIP-1α and MIP-1β increase macrophage trafficking ([17,30])
CCL2/MCP-1	macrophage inflammatory protein 1	chemokines	31.25−2000 pg/mL	31.0 pg/mL	100 pg/mL	336.88−522.59 pg/mL	macrophage infiltration is largely mediated by MCP1 and its receptor (CCL2). Chemokines regulate inflammation in the wound healing process ([17,24])

https://doi.org/10.1021/acsomega.1c05022
ACS Omega 2021, 6, 35538−35547

for osteogenic differentiation. The cells lost their fibroblast-like look and took on a more spherical, cuboidal form. Von Kossa staining was used to test DB-MSCs' capacity to differentiate into osteocytes when they were cultured under osteogenic differentiation conditions (Figure 3D). In cells grown under control conditions, no calcium accumulation was detected. Between osteogenic cells, there was intense black staining. BGLAP was never detected in cells grown in the control media (Figure 3C). DB-MSCs could be induced to differentiate into osteoblast-like cells, according to these findings. Collagen pellets with safranine O (positive stain) stained patches showed that *Decidua Basalis*-derived mesenchymal stromal cells were successfully differentiated to chondrocytes (Figure 3F) with each donor sample (n = 5), with respect to un-induced cultures (control) for comparison, and no differences were detected in control cells (Figure 3E).

Cells were grown consistently until the 10th passage level indicated higher colony-forming units in *Decidua Basalis* plates. Each plate (n = 5) of P(10) DB-MSCs showed a distinct colony-forming unit, proving the ability of the cell in the population to undergo "unlimited" division. The CFU analysis was depleted the clonogenic capacity of DB-MSCs of five donors (DB1 to DB5) as CFU 31, CFU 29, CFU 34, CFU 30, and CFU 36 respectively. The test values were compared to the colony-forming units of treated control (P2), which are closely matched with positive control value CFU 31 at the 10th passage level.

All studies were conducted by the criteria proposed by the International Society for Cellular Therapy (ISCT) to define human MSCs. These studies were found till 10th passage MSCs have an immunophenotype characteristic of MSCs and are capable of self-renewal. The metaphase chromosome spreads were analyzed in different batches of P(2) MSCs and P(10) MSCs wherein their karyotyping pattern was observed as normal. The genetic stability was analyzed for chromosomes after the conventional Giemsa banding for expanded MSCs was also observed as normal.

Chemokines play a vital role in the regulation of the wound curing processes. Additionally, it also shows a significant role in the stimulation and inhibition of angiogenesis, as well as the enrolment of growth factors producing inflammatory cells and cytokines to support wound curing. In this study, we emphasized the existence of growth factors, interleukins (ILs), chemokines, and tissue inhibitors of metalloproteinases (TIMPs) secreted by DB-MSCs, which are involved throughout the different stages of wound curing processes. Also, we explored the secretion profiling of GM-CSF, IL-7, IL-1alpha, IL-1beta, GRO-beta, TNF-alpha, EG-VEGF, PIGF-1, MIP-1alpha, MCP-1, ICAM-1, CTGF, CXCL 16, and RANTES for the possible application in the wound to suppress the devastating effects of impaired wound curing. Particularly, cytokines influence the function of immune cells; it includes interleukins, lymphokines, and other signaling molecules like interferons and tumor necrosis factors. They are documented according to their part in the wound curing process, which is enumerated in Table 2.

Inflammatory cytokines, also known as proinflammatory cytokines, are signaling molecules generated by immune cells such as helper T cells (Th), macrophages, and other cell types that induce inflammation. Interleukin-1 (IL-1), IL-12, and IL-18, as well as tumor necrosis factor alpha (TNF-), interferon gamma (IFN), and granulocyte-macrophage colony stimulating factor (GM-CSF), are key mediators of the innate immune response. Inflammatory cytokines are primarily generated by inflammatory processes and are involved in their up-regulation. In this study, proinflammatory cytokines such as IL-1beta, MCP-1, and ICAM were found up-regulated in 120 h compared to other chemokine and growth factors. Similarly, angiogenic growth factor EG-VEGF exhibits high levels of regulation. These studies hint at a contribution of MCP-1 in driving M1 macrophage polarization under certain pathological situations, and intercellular cell adhesion molecules (ICAM) are up-regulated by IL-6, but a direct mode of action was yet to be established. In fact, the release of pro-inflammatory cytokines might activate immune cells and cause them to produce and release more cytokines. As a result, when the phrase "cytokine storm" first appeared, it was used to describe inflammation as the abrupt release of cytokines to up-regulate an inflammatory process. Recent study suggests that in every immunological response, the simultaneous release of pro- and anti-inflammatory cytokines is vital.

The Wilcoxon test, also known as the rank sum test or the signed-rank test, compares two matched groups using a nonparametric statistical test. The assessment works by calculating and analyzing the differences between each pair of numbers. The Wilcoxon rank sum test is used to see if two populations have the same continuous distribution. The data must come from the same population and be paired, which is one of the prerequisites for using this technique of testing. The Wilcoxon signed-rank test assumes that the magnitudes and signs of differences between paired observations contain information. The Wilcoxon test was used to examine the differences between each pair and their differences for 72 and 120 h cytokine values. The null hypothesis was tested between the two populations for the cytokines/chemokines/growth factors M-CSF, IL-7, IL-1alpha, IL-1beta, GRO-beta, TNF-alpha, EG-VEGF, PIGF-1, MIP-1alpha, MCP-1, ICAM-1, CTGF, CXCL 16, and RANTES involved in wound healing and secretion concentration in 72 and 120 h. According to the Wilcoxon signed-rank test, the null hypothesis of 72 and 120 h has the same continuous distribution.

For the cytokines ICAM-1, CTGF, CXCL 16, and RANTES, the data for chosen cytokine profiling is examined for secreted cytokine concentrations in ng/mL. Stack column statistical analysis is expressed as mean SEM (Figure 4C), while interleaved column statistical analysis is expressed as mean SD (Figure 4D). The column statistics of 72 h had a mean of 130 ng/mL SD 200 of SD error 99, with a minimum value of 5.8 ng/mL and a high value of 420 ng/mL. $P < 0.05$ indicates that the P-value (two-tailed) is statistically significant. Similarly, the column statistics of 120 h had a minimum value of 8.2 ng/mL and a maximum value of 510 ng/mL, with a mean of 160 ng/mL SD 230 of SD error 120 and a mean of 160 ng/mL SD 230 of SD error 120.

The secreted cytokine concentrations in pg/ml for the cytokines GM-CSF, IL-7, IL-1alpha, IL-1beta, GRO-beta, TNF-alpha, EG-VEGF, PIGF-1, MIP-1alpha, and MCP-1 are examined using cytokine profiling data. Stack column statistical analysis is expressed as mean SEM (Figure 4A), while interleaved column statistical analysis is expressed as mean SD (Figure 4B). The column statistics of 72 h had a mean of 73 ng/mL SD 96 of SD error 30 and a low value of 4.9 ng/mL and a maximum value of 300 ng/mL. The statistical significance ($P < 0.05$) of the P-value (two-tailed) is 0.0395. Similarly, the column statistics of 120 h had a mean of 100 ng/mL SD 140 of SD error 43, with a low value of 6.2 ng/mL and

https://doi.org/10.1021/acsomega.1c05022
ACS Omega 2021, 6, 35538−35547

a high value of 420 ng/mL. The statistical significance ($P < 0.05$) of the P-value (two-tailed) is 0.0429.

CONCLUSIONS

The *in vitro* clinical characterization and large scale production of DB-MSCs were optimized in this study to fulfill therapeutic applications. Furthermore, the presence of critical growth factors and cytokines that are specifically adapted to help in wound healing was reviewed. In addition, the paracrine secretion properties of MSCs and the animal toxicity study that would determine the clinical toxicity associated with the therapeutic product, adequate safety margin, dosage limitations, and route of administration to ensure systemic dissemination of MSCs for intended therapeutic usage warrant further investigation.

MATERIALS AND METHODS

Material Source. With parental consent and institutional committee approval, the maternal component of the placenta: *Decidua Basalis* ($n = 5$) was taken from a caesarean section. The collected samples were refrigerated in Dulbecco's phosphate-buffered saline (DPBS) with 15 units/mL penicillin, 60 g/mL gentamycin, 0.125 mg/mL cefoperazone sodium, and 1.5 mg/mL amphotericin B and promptly transported to the lab.

Cell Isolation. All tissue culture activities were carried out in a cleanroom class 1000 environment, and the study complied with the established cGLP and cGMP norms. In the laboratory, under the Class II Type A2 biosafety cabinet, the *Decidua Basalis* region of the placenta, weighing 10−15 g, was manually dissected from the maternal surface and cleaned thoroughly with in-house DPBS before being translucently milled and rinsed until the fluid was blood-free. The tissue pellet was digested with 0.25% Trypsin EDTA, 10 units/mL penicillin, 50 g/mL gentamycin, 0.125 mg/mL cefoperazone sodium, and 0.5 mg/mL amphotericin B in a 5% CO_2 incubator at 37 °C for 1.5 h after centrifugation at 210*g* for 10 min. Following centrifugation, the cell suspension, as well as the separated, filtered chunks, were planted in the range of 4−6 g per T75 flask, (depending on chunk size) kept in a 5% CO_2 incubator for 4−5 days at 37 ° C, subsequently, in which renewed media were replaced into the flasks.

Cell Culture. MSC culture medium consisted of single-cell suspensions of *Decidua Basalis* grown in DMEM/F12+ (Gibco, USA) and 10% fetal bovine serum (Gibco, USA) augmented with 1.5 ng/mL bFGF (Sigma, USA). The tissue culture grade T-75 flasks were coated with 1% gelatine and left in a moistened environment of 5% CO_2 at 37 ° C for 30 min and were used to plate the cells and chunks (Nunc, Denmark). Non-adhering cells were eliminated after 7 days, and the media was replaced. Adherent cells were removed using trypsin/EDTA for 5 min at 37 °C and extended in culture flasks after they reached confluence, and the basic data of scale-up *Decidua Basalis* MSCs are tabulated in Table 3.

Cell Seeding Density Vs Passages. Harvested cells at P(0) were plated in T-175 cell culture flasks (New York, USA) for P(1) and HYPER flasks for P(2) at a density of 3000 cells/cm^2 (Corning, NY, USA). In T-175 tissue culture flasks, 3000 cells/cm^2 were plated at P(3) to P(10). The acquired cells were laid in a cryoprotectant solution comprising 90% medium and 10% dimethyl sulfoxide (DMSO) and preserved in a liquid nitrogen tank's vapor phase until utilized.

Table 3. Basic Data of Scaled-up *Decidua Basalis* MSCs

	DB1	DB2	DB3	DB4	DB5
total weight of DB seeded (g)	4.67	4.32	4.8	5.96	4.45
seeding density (g)	0.58	0.54	0.60	0.75	0.56
P(0) culture period (days)	16	15	15	15	18
P(0) harvested cells [($\times 10^6$ cells)/8T-75]	9.9	10.3	13.55	14.7	9.8
P(0) harvested cells ($\times 10^4$ cells/cm^2)	1.65	1.72	2.26	2.45	1.63
viability (%)	96.0	96.1	97.0	97.3	96.0
no. of flasks used (T175) at P(1)	19	20	26	28	19
total yield of cells at P1 ($\times 10^8$)	1.23	1.37	2.22	2.6	1.2
harvested cells ($\times 10^4$/cm^2)	3.71	4.00	4.91	5.31	3.66
duration of P(1) culture (days)	5	5	5	5	6
no. of flasks used at P(2) (Hyperflask)	24	27	43	50	23
total yield of cells at P(2) ($\times 10^9$)	1.71	2.00	3.66	4.74	1.60
harvested cells ($\times 10^4$/cm^2)	4.19	4.36	4.94	5.47	4.01
duration of P(2) culture (days)	10	10	10	9	11
exposed culture media (L)	26.13	29.28	47.32	55.51	25.47
no. of T175 flasks used at P10	2	2	2	2	2
total yield of cells at P(10) ($\times 10^6$)	14	15	18.2	19.6	13.8
harvested cells ($\times 10^4$/cm^2)	4.00	4.29	5.20	5.60	3.94
duration of P(10) culture (days)	6	6	6	6	6

Phenotyping and Purity Analysis. The harvested cells were analyzed for *Decidua Basalis* immunophenotypic characterization, and as per optimization, the protocol with 10,000 cells was incubated with fluorochromes conjugated anti-human primary antibodies. *Decidua Basalis* cells were stained with antibodies CD90-FITC (2 μL), CD73-APC (5 μL), CD45-FITC (20 μL), CD34-PE (20 μL), CD19 (20 μL), CD14 (20 μL), CD133 (20 μL), CD105-PE (20 μL), CD166 (5 μL), and HLA-DR (5 μL) (BD Biosciences, USA). Cells were incubated over equal concentrations of FITC- (5 μL), PE- (5 μL), PercpCyc.5.5 (5 μL), and APC- (5 μL) coupled with mouse IgG isotype secondary antibodies (isotype controls). After 10 min of incubation at 37 °C, the cells were attained by a flow cytometer (BD Biosciences, USA). Nearly, 10^4 events were observed and analyzed by applying Cell Quest Pro software (BD Biosciences, USA).

Tri-Lineage Differentiation. The propensity for tri-lineage differentiation of *Decidua Basalis* derived MSCs harvested under corresponding culture conditions, *viz.*, osteocyte, adipocyte, and chondrocyte differentiations, was investigated,[13−15] and images were documented with an Olympus microscope (Olympus, Japan).

Colony Forming Unit (CFU) Assay. The clonogenic capacity of DB-MSCs was estimated with a previously reported procedure,[13] and the effectiveness on the survival and proliferation of cells were documented.

Chromosomal Analysis. Karyotyping of final harvested cells was carried out using a standard Giemsa banding procedure as previously described with some modifications.[13,14]

https://doi.org/10.1021/acsomega.1c05022
ACS Omega 2021, 6, 35538−35547

Cytokine Quantitative Assessment. The cell culture supernatant was collected from T175 tissue culture flasks with an initial seeding density of 3000 cells/cm^2 at the 10th passage level of the sample at 72 and 90 h for sample extraction and analyzed for quantitative analysis. Each cytokine was assayed using a specialized enzyme linked immunosorbent assay (ELISA) kit (R&D Systems). The assay is based on quantitative sandwich enzyme immunoassay methodology, which incorporates pre-coating a microplate with an antibody specific for each cytokine, and the analysis was repeated thrice in parallel. Upon 30 min on ice, the samples were re-suspended in a Triton X-100 lysis buffer (20 mM Hepes, pH 7.4, 150 mM NaCl, 10% glycerol, 1% Triton X-100, and complete protease inhibitor (CPI) combination) and centrifuged for 30 min at 14,000*g* at 4 ° C to eliminate debris prior to the ELISA test. The ELISA tests were carried out as per the maker's guidelines. The Bradford protein test was performed to quantify the total protein content of each sample, which was then utilized to normalize the total cytokine concentration. The software used to estimate ELISA data interpretation was Magellan from Tecan Inc., USA.

Precision. To quantify intra-assay accuracy, known concentrations of samples were evaluated on one plate. Similarly, to determine inter-assay precision, three samples of known concentration were examined in independent assays. Whereas, CV (%) = SD/mean × 100. The threshold for the intra-assay is CV < 8%, and that for the inter-assay is CV < 10%.

Data Analysis and Statistics. Data are expressed as mean ± standard deviation for illustration. To assess the null hypothesis of two populations with the same continuous distribution, the Wilcoxon rank sum test is employed. The base norms are essential in applying this method to analyze the data. The Wilcoxon signed-rank test statistical analysis was analyzed by the use of SPSS software version 26 (IBM SPSS software, USA). The threshold for arithmetical impact was fixed at $p < 0.05$.

Data for interleaved column statistical analysis are expressed as mean ± SD, and data for stacked column statistical analysis are shown as mean ± SEM. Difference and comparison between groups were evaluated by column statistics followed by *t*-test using GraphPad Prism software version 3.0 (GraphPad Software, USA). $P < 0.05$ was agreed as the statistical significance value.

AUTHOR INFORMATION

Corresponding Author

Veeramanikandan Veeramani − *PG and Research Centre in Microbiology, MGR College, Hosur 635130 Tamil Nadu, India;* orcid.org/0000-0002-6235-1223; Email: vra.manikandan@gmail.com

Authors

Priya Subramani − *PG and Research Centre in Microbiology, MGR College, Hosur 635130 Tamil Nadu, India*

Jaianand Kannaiyan − *Research and Development, CellCure Therapeutics, Madurai 624217 Tamil Nadu, India*

Jothi Ramalingam Rajabathar − *Chemistry Department, College of Science, King Saud University, Riyadh 11451, Saudi Arabia;* orcid.org/0000-0001-6205-3317

Prema Paulpandian − *PG and Research Department of Zoology, VHN Senthikumara Nadar College, Virudhunagar 626001 Tamil Nadu, India*

Ramesh Kumar Kamatchi − *PG and Research Department of Zoology, Vivekananda College, Madurai 624217 Tamil Nadu, India*

Balaji Paulraj − *PG and Research Centre in Biotechnology, MGR College, Hosur 635130 Tamil Nadu, India*

Hamad A. Al-Lohedan − *Chemistry Department, College of Science, King Saud University, Riyadh 11451, Saudi Arabia*

Selvaraj Arokiyaraj − *Department of Food Science and Biotechnology, Sejong University, 635130 Seoul, South Korea*

Complete contact information is available at: https://pubs.acs.org/10.1021/acsomega.1c05022

Notes

The authors declare no competing financial interest.

ACKNOWLEDGMENTS

We wish to acknowledge CellCure Therapeutics for the institutional research board (NCP/IAEC/2018-19/11) and Nandha College of Pharmacy, Erode, for the study support as per the guidelines of Institutional Animal Ethical Committee 9688/PO/Re/S/02/CPCSEA. This work was funded by the Researchers Supporting Project number (RSP-2021/54), King Saud University, Riyadh, Saudi Arabia.

REFERENCES

(1) Gurtner, G. C.; Werner, S.; Barrandon, Y.; Longaker, M. T. Wound repair and regeneration. *Nature* **2008**, *453*, 314.

(2) Guo, S.; DiPietro, L. A. Factors affecting wound healing. *J. Dent. Res.* **2010**, *89*, 219−229.

(3) Serra, M. B.; Barroso, W. A.; da Silva, N. N.; Silva, S. D. N.; Borges, A. C. R.; Abreu, I. C.; Borges, M. O. D. R. From Inflammation to Current and Alternative Therapies Involved in Wound Healing. *Int. J. Inflammation* **2017**, *2017*, 1.

(4) Schultz, G. S.; Wysocki, A. Interactions between extracellular matrix and growth factors in wound healing. *Wound Repair Regener.* **2009**, *17*, 153−162.

(5) Barrientos, S.; Stojadinovic, O.; Golinko, M. S.; Brem, H.; Tomic-Canic, M. Growth factors and cytokines in wound healing. *Wound Repair Regener.* **2008**, *16*, 585−601.

(6) Han, G.; Ceilley, R. Chronic wound healing: a review of current management and treatments. *Adv. Ther.* **2017**, *34*, 599−610.

(7) Masoudi, E. A.; Ribas, J.; Kaushik, G.; Leijten, J.; Khademhosseini, A. Platelet-rich blood derivatives for stem cell-based tissue engineering and regeneration. *Curr. Stem Cell Rep.* **2016**, *2*, 33−42.

(8) Ud-Din, S.; Sebastian, A.; Giddings, P.; Colthurst, J.; Whiteside, S.; Morris, J.; Nuccitelli, R.; Pullar, C.; Baguneid, M.; Bayat, A. Angiogenesis is induced and wound size is reduced by electrical stimulation in an acute wound healing model in human skin. *PLoS One* **2015**, *10*, No. e0124502.

(9) Brantley, J. N.; Verla, T. D. Use of placental membranes for the treatment of chronic diabetic foot ulcers. *Adv. Wound Care.* **2015**, *4*, 545−559.

(10) Gupta, A.; Kedige, S. D.; Jain, K. Amnion and Chorion Membranes: Potential Stem Cell Reservoir with Wide Applications in Periodontics. *Int. J. Biomater.* **2015**, *2015*, 1.

(11) Chibbar, R.; Miller, F. D.; Mitchell, B. F. Synthesis of oxytocin in amnion, chorion, and decidua may influence the timing of human parturition. *J. Clin. Invest.* **1993**, *91*, 185−192.

(12) Riboldi, M.; Simon, C. Extraembryonic tissues as a source of stem cells. *Gynecol. Endocrinol.* **2009**, *25*, 351−355.

(13) Kannaiyan, J.; Paulraj, B. Clinical Prospects of Scale-Up Foetal Wharton's Jelly derived Multipotent Stromal Cells to fulfil the Therapeutic Demands. *Int. J. Pharma Bio Sci.* **2015**, *6*, 882−894.

(14) Kannaiyan, J.; Paulraj, B. Isolation, Characterization, and Scale-Up of Foetal Amniotic Membrane Derived Multipotent Stromal Cells

for Therapeutic Applications. *Int. J. Pharma Bio Sci.* **2015**, *6*, 376−385.
(15) Kannaiyan, J.; Muthukutty, P.; Iqbal, M. D. T.; Paulraj, B. Villous Chorion: A potential source for pluripotent-like stromal cells. *J. Nat. Sci. Biol. Med.* **2017**, *8*, 221−228.
(16) Leuning, D. G.; Beijer, N. R. M.; du Fossé, N. A.; Vermeulen, S.; Lievers, E.; van Kooten, C.; Rabelink, T. J.; de Boer, J. The cytokine secretion profile of mesenchymal stromal cells is determined by surface structure of the microenvironment. *Sci. Rep.* **2018**, *8*, 7716.
(17) Al-Shaibani, M. B. H.; Wang, X. N.; Lovat, P. E.; Dickinson, A. M. Cellular therapy for wounds: Applications of mesenchymal stem cells in wound healing. *Wound Healing-New insights Ancient Challenges* **2016**, 99.
(18) Park, C. W.; Kim, K. S.; Bae, S.; Son, H. K.; Myung, P. K.; Hong, H. J.; Kim, H. Cytokine secretion profiling of human mesenchymal stem cells by antibody array. *Int. J. Stem Cells* **2009**, *2*, 59−68.
(19) Bartlett, A.; Sanders, A. J.; Ruge, F.; Harding, K. G.; Jiang, W. G. Potential implications of interleukin-7 in chronic wound healing. *Exp. Ther. Med.* **2016**, *12*, 33−40.
(20) Kyurkchiev, D.; Bochev, I.; Ivanova-Todorova, E.; Mourdjeva, M.; Oreshkova, T.; Belemezova, K.; Kyurkchiev, S. Secretion of immunoregulatory cytokines by mesenchymal stem cells. *World J. Stem Cells* **2014**, *26*, 552−570.
(21) Redondo-Castro, E.; Cunningham, C.; Miller, J.; Martuscelli, L.; Aoulad-Ali, S.; Rothwell, N. J.; Kielty, C. M.; Allan, S. M.; Pinteaux, E. Interleukin-1 primes human mesenchymal stem cells towards an anti-inflammatory and pro-trophic phenotype *in vitro*. *Stem Cell Res. Ther.* **2017**, *8*, 79.
(22) Broekman, W.; Amatngalim, G. D.; de Mooij-Eijk, Y.; Oostendorp, J.; Roelofs, H.; Taube, C.; Stolk, J.; Hiemstra, P. S. TNF-α and IL-1β-activated human mesenchymal stromal cells increase airway epithelial wound healing *in vitro* via activation of the epidermal growth factor receptor. *Respir. Res.* **2016**, *17*, 3.
(23) Lee, C. H.; Shah, B.; Moioli, E. K.; Mao, J. J. CTGF directs fibroblast differentiation from human mesenchymal stem/stromal cells and defines connective tissue healing in a rodent injury model. *J. Clin. Invest.* **2010**, *120*, 3340−3349.
(24) Galindo, L. T.; Thais, R. M. F.; Patricia, S.; Carolina, B. A.; Caroline, M. M.; Niels, S. C.; Marimelia, A. Mesenchymal Stem Cell Therapy Modulates the Inflammatory Response in Experimental Traumatic Brain Injury. *Neurol. Res. Int.* **2011**, *2011*, 1.
(25) Schinkothe, T.; Bloch, W.; Schmid, A. *In-vitro* secreting profile of human mesenchymal stem cells. *Stem Cells Dev.* **2008**, *17*, 199−206.
(26) Ziaei, R.; Ayatollahi, M.; Yaghobi, R.; Sahraeian, Z.; Zarghami, N. Involvement of TNF-α in differential gene expression pattern of CXCR4 on human marrow-derived mesenchymal stem cells. *Mol. Biol. Rep.* **2014**, *41*, 1059−1066.
(27) Watt, S. M.; Gullo, F.; van der Garde, M.; Markeson, D.; Camicia, R.; Khoo, C. P.; Zwaginga, J. J. The angogenic properties of mesenchymal stem cell/Stromal cells and their therapeutic potential. *Br. Med. Bull.* **2013**, *108*, 25−53.
(28) Maxson, S.; Lopez, E. A.; Yoo, D.; Danilkovitch-Miagkova, A.; Leroux, M. A. Concise review: role of mesenchymal stem cells in wound repair. *Stem Cells Transl. Med.* **2012**, *1*, 142−149.
(29) Park, S. J.; Kim, K. J.; Kim, W. U.; Cho, C. S. Interaction of mesenchymal stem cells with fibroblast-like synoviocytes via cadherin-11 promotes angiogenesis by enhanced secretion of placental growth factor. *J. Immunol.* **2014**, *192*, 3003−3010.
(30) Rice, C. M.; Scolding, N. J. Adult human mesenchymal cells proliferate and migrate in response to chemokines expressed in demyelination. *Cell Adh. Migr.* **2010**, *4*, 235−240.

https://doi.org/10.1021/acsomega.1c05022
ACS Omega 2021, 6, 35538−35547